Analysis and Refinement of a Method for Numerically Modeling Deep-Penetration Welding Processes Using Geometric Constraints

S.G. Lambrakos and J. Milewski

A detailed analysis and refinement of a method of numerically modeling deep-penetration welding processes using geometric constraints based on boundary information obtained experimentally is presented. The general features of the numerical method have been described previously. This paper considers issues concerning accurate numerical calculation of temperature and velocity fields in regions of the melt pool where the flow of fluid is characterized by quasi-stationary Stokes flow. It is this region of the melt pool that is closest to the heat-affected zone and that represents a significant fraction of the fusion zone.

Keywords
deep-penetration, geometric constraints, numerical modeling

1. Introduction

IN A previous paper (Ref 1), the present authors introduced a numerical model and an associated collection of numerical methods for calculating structures that can occur in deep-penetration welding processes (i.e., laser or electron beam). That report described the general features of the numerical model, that is, the underlying physical model and the associated numerical methods. It also provided a general survey of possible extensions of the numerical model that are possible in principle because of two factors: (1) the inherent physical character of the deep-penetration welding process and (2) the flexibility inherent in the general formalism of the SIMPLE algorithm with respect to its modification or extension for modeling the deep-penetration welding process.

In another paper (Ref 2), we further discussed numerical methods for effecting calculations with the model. That report introduced two procedures for the inclusion of experimental information concerning steady-state weld-pool shape into the model system. These procedures entail the application of constraints and the deduction of effective keyhole shape via an inverse mapping procedure. A feature of the procedure for imposing constraints is that it tends to compensate for either the unavailability of experimental measurements of material properties or gaps in knowledge concerning the general character of the keyhole. A feature of the inverse mapping procedure is that it tends to compensate for error propagation within the solution domain due to coarse-grid discretization of the solution in regions close to the keyhole. In the present paper, the two procedures for implementing constraints that are presented in Ref 2 are combined within a more refined reformulation of the geometric-constraints method.

This paper considers issues concerning accurate numerical calculation of temperature and velocity fields in regions of the melt pool where the flow of fluid is characterized by quasi-steady Stokes flow. The underlying motivation of our present development is that it is *transport* in these regions of the melt pool which couples most *strongly* and *directly* to the heat-affected zone (HAZ) and which, because of the rapid onset of viscous effects, represents a significant fraction of the fusion zone (FZ). The physical characteristics of all other regions of the melt pool, as well as the keyhole itself, are considered with respect to the relative strength of their coupling to regions of the melt pool that are close to the solidification boundary and within the Stokes-flow regime. Regions of the melt pool that are close to the keyhole present a particular problem because of the sharp rise in temperature. With respect to numerical discretization, these regions can be characterized effectively as numerical singularities resulting from the type of stiffness that occurs in the integration of shocklike structures. However, regions of the melt pool that are close to the solidification boundary are characterized by fluid properties, which provide a means of overcoming any ill-conditioning due to the numerically singular character of regions near the keyhole and a more accurate specification of the flow. Because the character of the flow in regions that are close to the trailing solidification boundary is not coupled to the details of the character of the flow in regions near the keyhole, a well-posed input condition is a set of upstream boundary values of the temperature and fluid-flow fields. The reformulation of the geometric-constraints method presented in this paper entails the specification of a consistent set of upstream boundary values of temperature and flow velocity rather than explicit specification of the beam energy source.

S.G. Lambrakos, Materials Science and Technology Division, Naval Research Laboratory, Washington, DC 20375-5000, USA; **J. Milewski,** Los Alamos National Laboratory, Los Alamos, NM, USA.

2. Physical Model of Deep-Penetration Welding

The general features of our numerical model are described in Ref 1 and 2. What is presented here is actually a refinement of the model based on its extension to include geometric-constraint information. In the context of using geometric constraints, it is the solidification boundary and top surface boundary that determine the solution, rather than the boundary corresponding to the vapor-liquid interface associated with the keyhole. Given this, it follows that the flow characteristics of the liquid in regions of the melt pool near the solid-liquid

boundary must be modeled accurately. The keyhole boundary or keyhole source term, depending on the fashion of implementation, is only used to adjust the characteristically monotonic flow field along the top surface and solidification boundaries. Therefore, in the present model, it is not considered a true boundary of the system or, more precisely, of the solution domain. The present model adopts the approximation that the flow character of the liquid region is mostly that of quasi-steady Stokes flow (Ref 3, 4). The significance of this approximation with respect to numerical modeling of the weld melt pool is discussed in the next section.

The model system to be specified is characterized by quasi-steady mass, energy, and momentum transport in a coordinate system that is fixed in the reference frame of a moving beam energy source, that is, an electron or laser beam. The Boussinesq approximation (Ref 5) is applied to the system of transport equations underlying the numerical model. A schematic of the model system is shown in Fig. 1. The boundaries of the model system are defined, at each time step, by the sides of a finite-sized rectangular region containing the beam and by the temperature of vaporization isotherm, which is taken to represent the vapor-liquid boundary of the keyhole. Outflow boundary conditions are imposed on all boundaries other than that of the keyhole.

The system is assumed to be symmetric about the xz-face at $y = 0$ (see Fig. 1); thus, only one-half of the system is modeled. The equations of transport governing the model system are as follows. The equation of energy transport is:

$$\frac{\partial T}{\partial t} + \nabla \cdot [\mathbf{U}T] + \delta_{1j} V_B \frac{\partial T}{\partial x_j} = \kappa(T)\nabla^2 T(\mathbf{x},t) + \nabla \cdot \mathbf{q} \qquad \text{(Eq 1)}$$

where

$$\kappa(T) = \frac{k(T)}{\rho(T) C_p(T)} \qquad \text{(Eq 2)}$$

and

$$\nabla \cdot \mathbf{q} = \sum_{l=1}^{N_3} \nabla \cdot \mathbf{q}_l \qquad \text{(Eq 3)}$$

The term $\nabla \cdot \mathbf{q}$ represents the total energy transferred into the system from different types of sources. The equation of momentum transport is:

$$\frac{\partial U_j}{\partial t} = \nu(T)\nabla^2 U_j - \frac{1}{\rho(T)} \frac{\partial P}{\partial x_j} \qquad \text{(Eq 4)}$$

where

$$\nu(T) = \frac{\mu(T)}{\rho(T)} \qquad \text{(Eq 5)}$$

and $j = 1, 2, 3$ denotes the Cartesian coordinates x, y, and z, respectively. Lastly, the equation of mass transport is:

$$\nabla \cdot \mathbf{U} = 0 \qquad \text{(Eq 6)}$$

The quantity $\mathbf{U} = (U_1, U_2, U_3) = (u, v, w)$ is the velocity field at a given point, and $\mathbf{x} = (x_1, x_2, x_3) = (x, y, z)$ is the Cartesian coordinate of that point. The quantity V_B is the speed of the beam, moving in the direction of increasing x, and δ_{ij} is the Kronecker delta function. The quantity P is the pressure at a given point, and T is the temperature. In our model, the density $\rho(T)$, coefficient of viscosity $\mu(T)$, conductivity $k(T)$, and heat capacity $C_p(T)$ are functions of temperature T. The thermal coefficient of surface tension is given by:

$$\frac{\partial \gamma}{\partial T} = -A_n f_s(x,y) \qquad \text{(Eq 7)}$$

where A_n is a constant and $f_s(x, y)$ is a two-dimensional modulation function whose form is specified according to experimental information about melt-pool shape. The quantity given by Eq 7, which is formally equivalent to the coefficient of surface tension, is for the purpose of lumping the influence of phenomena occurring in the vicinity of the keyhole and at the top surface of the melt pool, which are not included explicitly in the model system. Further discussion concerning this quantity is given in Ref 2. It is to be noted, however, that this function provides a means of including experimentally obtained information concerning the shape of the melt pool.

It might be noted that Eq 4 is given in vector-component form, whereas Eq 1 and 6 are given in vector form. This difference of representation is only for purposes of notational consistency with respect to the subsequent development given in section 5. In addition, we have purposefully not included, for the sake of clarity, the effects of latent heat of fusion and of fluid flow due to buoyancy, which represent additional terms to Eq 1 and 4, respectively. These effects, although significant with respect to quantitative analysis, are not relevant within the context of our present development, which concerns a general analysis and refinement of the geometric-constraints method (Ref 2). It should be noted, however, that the inclusion of these effects via the addition of terms to the equations of transport does not alter any of the derivations presented in this report.

In Eq 1, the influence of convection is represented by two terms: one containing $\mathbf{U}$ and one containing V_B. This representation follows because the flow field associated with the convection term in the energy transport equation (Eq 1) is defined with respect to an origin that is fixed in the workpiece. The component of the flow field parallel to the direction of the motion of the beam is therefore $\rho(u + V_B)$; however, the dependent variables of the momentum transfer equations (u, v, w) are the velocities relative to an origin that is stationary with respect to the beam. The weighting coefficients for the discretization of Eq 1 as defined by the SIMPLE algorithm (Ref 6) are modified to take into account this representation. The properties of the SIMPLE method with respect to solving Eq 4 are discussed in section 5. In addition, although we have adopted the weighting coefficients that are employed by the SIMPLE algo-

rithm, the numerical procedure employed here is different and is structured for the particular problem considered in this study.

At the keyhole liquid-vapor interface, the boundary conditions on the momentum transfer equations are those of a no-slip boundary. That is, the component of the velocity, in the reference frame of the workpiece, normal to the interface is zero:

$$\mathbf{U} \cdot \hat{\mathbf{n}} + \mathbf{V_B} \cdot \hat{\mathbf{n}} = 0 \qquad \text{(Eq 8)}$$

where $\hat{\mathbf{n}}$ is the unit normal to the keyhole liquid-vapor boundary and $\mathbf{V_B}$ is the velocity of the beam with respect to the workpiece and is in the x-direction. Another boundary on the molten region is defined by the solid-liquid interface. The boundary condition on this boundary is specified in our model according to:

$$U_j = -\delta_{1j} V_B, \quad \text{if } T < T_M \qquad \text{(Eq 9)}$$

Note that according to this specification, the set of all nodes having temperature values less than T_M includes both boundary and exterior points of the melt pool.

Note: A significant feature of the analysis and geometric-constraints method presented in this paper is the explicit separation of upstream and downstream boundary conditions according to their relative weighting on the flow field within the weld melt pool. Accordingly, the boundary condition that is defined by Eq 8, although formally a boundary condition on the model system, is not adopted within our present development as a boundary condition on the *solution domain.* A point of emphasis in the analysis, based on the inherent monotonicity of the temperature and flow fields in the weld melt pool, is that the inclusion of geometric-constraint information imposes the necessity of having to make choices with respect to the inclusion of boundary conditions. Equations 1 to 9 are sufficient for a unique specification of the system. Inclusion of geometric-constraint information, however, implies an overspecification of the system. Depending on the type of geometric-constraint information included, it is necessary to make a choice between either upstream boundary values (e.g., Eq 8) or downstream boundary values for specification of the system.

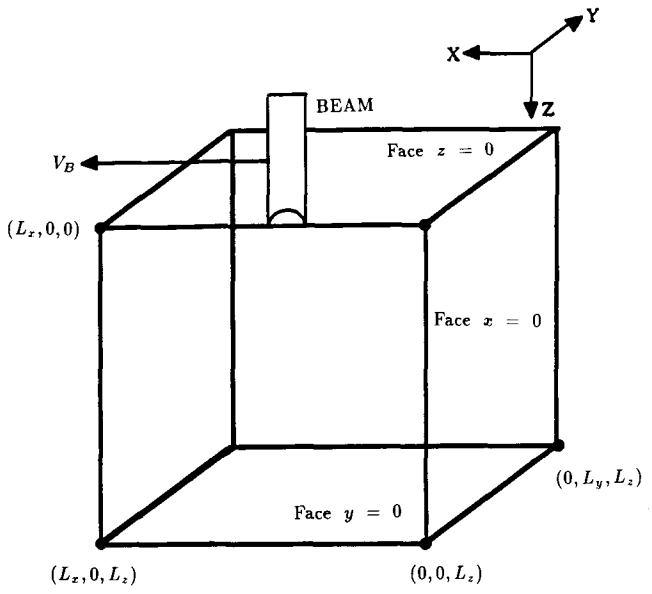

Fig. 1 Schematic of model system showing relative coordinates of system boundaries

3. Discussion of Computational Issues

This section delineates physical properties and practical considerations influencing our choice of numerical methods for modeling deep-penetration welding processes occurring within regions that are close to the solidification boundary. Regions of the system that are relatively close to the vapor-liquid boundary defining the keyhole are characterized by large temperature gradients. Consequently, numerical discretization of the differential equations of transport over the solution domain which encloses the combined system of regions that are close and regions not close to the keyhole can result in a discretized system that is stiff (Ref 7) and therefore ill-conditioned for accurately calculating the coupling between these regions. This type of error propagation tends not to be significant for numerical modeling procedures that employ information concerning the shape of the solid-liquid boundary (Ref 2). These procedures tend to damp out errors that may result from either a time-averaged estimate of the keyhole boundary or discretization error.

Mass, momentum, and energy transport are characterized by two types of upstream influence or weighting. First, for regions very close to the keyhole, there is an upstream weighting relative to the center of the keyhole. Second, there is an upstream weighting relative to the direction of the motion of the beam. This upstream weighting increases with the degree of proximity to the keyhole and is due to (1) the relative motion of the beam with respect to the workpiece and (2) the flow of fluid above the top surface of the workpiece and in the direction opposite to that of beam motion. These two types of upstream weighting imply a monotonicity of the flow field.

The top-surface boundary of the model system represents a major influence on the character of the solution within the solution domain. The nature of the solution in regions that are both near to the top boundary and near to the keyhole boundary, however, poses a numerical sensitivity problem. This sensitivity problem results from the sharp rise in temperature which numerically is analogous to shock structures occurring in cases of rapid momentum transport and which is effectively discontinuous. Calculation of temperature gradients in this *singular* region via numerical finite-differences can result in large errors. This is significant because, considering the partially parabolic character of the system, it is the keyhole and top surface boundaries which essentially *drive* the solution in the absence of any additional information concerning the solidification boundary.

No matter what the character of the flow field in regions close to the keyhole or at points within the liquid somewhat removed from the solidification boundary, the Reynolds number is very small for regions of the melt pool close to the solidification boundary. Therefore, for regions of the melt pool close to the solidification boundary, the velocity field is specified by Stoke's equation (i.e., Eq 4).

The keyhole is very small relative to the total volume of the steady-state melt pool. That is to say, the total area of the surface defined by the vapor-liquid boundary is extremely small relative to the total area of the surface defined by the union of the steady-state solidification boundary extending into the workpiece and the planar boundary formed by the intersection of the molten pool and top surface plane. This large difference in total surface area has mathematical implications with respect to the solution domain. It implies that the keyhole, although an energy source with respect to the temperature field, can be considered as effectively not being a boundary of the solution domain.

The solution domain over which the velocity field is to be specified is *closed* in the mathematical sense. This property provides additional conditions with respect to which a solution can be determined. This closed-boundary perspective may not be intuitively apparent when considering the problem from the standpoint of a keyhole moving through a liquid. The deep-penetration welding problem, when posed from an open-boundary perspective, tends to overlook the existence of the solidification boundary as a *true* system boundary and considers both liquid and solid regions as part of an unbounded fluid domain, which is simply not the case.

Unsteady or turbulent flow structures occurring in regions close to the keyhole or at points within the liquid somewhat removed from the solidification boundary are weakly coupled to the *trailing* solidification boundary, whose shape remains effectively fixed. An analysis of the coupling between the leading and trailing boundary is given in section 6.

4. Boundary Conditions

This section specifies the boundary conditions on each face of the sample with respect to temperature and velocity. In the present development, the model system is that of a portion of the workpiece within which the entire melt pool is contained. This condition is consistent with the requirement that the model system include a liquid region extending over a finite and closed domain. The outflow boundary conditions for the temperature field are based on a linear extrapolation.

Boundary conditions on the xy-face at $z = 0$ are:

$$\frac{\partial T}{\partial z} = 0 \qquad \text{(Eq 10a)}$$

$$\mu \frac{\partial u}{\partial z} = -\frac{\partial \gamma}{\partial T}\frac{\partial T}{\partial x} \text{ and } \mu \frac{\partial v}{\partial z} = -\frac{\partial \gamma}{\partial T}\frac{\partial T}{\partial y}, \text{ if } T_M \le T \le T_G \qquad \text{(Eq 10b)}$$

$$u = -V_B \text{ and } v = 0, \text{ otherwise} \qquad \text{(Eq 10c)}$$

and

$$w = 0 \qquad \text{(Eq 10d)}$$

The quantity $\partial\gamma/\partial T$ is the thermal coefficient of surface tension.

Boundary conditions on the xy-face at $z = L_z$ and at time $t + \Delta t$ are:

$$T(x, y, L_z, t + \Delta t) = [\max\left[T_A, \frac{T(x, y, L_z - \Delta l, t)^2}{T(x, y, L_z - 2\Delta l, t)}\right] \qquad \text{(Eq 11a)}$$

$$\mu \frac{\partial u}{\partial z} = -\frac{\partial \gamma}{\partial T}\frac{\partial T}{\partial x} \text{ and } \mu \frac{\partial v}{\partial z} = -\frac{\partial \gamma}{\partial T}\frac{\partial T}{\partial y}, \text{ if } T_M \le T \le T_G \qquad \text{(Eq 11b)}$$

$$u = -V_B \text{ and } v = 0, \text{ otherwise} \qquad \text{(Eq 11c)}$$

and

$$w = 0 \qquad \text{(Eq 11d)}$$

Boundary conditions on the xz-face at $y = 0$ are:

$$\frac{\partial T}{\partial y} = 0 \qquad \text{(Eq 12a)}$$

$$\frac{\partial u}{\partial y} = 0, \quad v = 0, \quad \text{and} \quad \frac{\partial w}{\partial y} = 0 \qquad \text{(Eq 12b)}$$

Boundary conditions on the xz-face at $y = L_y$ and at time $t + \Delta t$ are:

$$T(x, L_y, z, t + \Delta t) = \max\left[T_A, \frac{T(x, L_y - \Delta l, z, t)^2}{T(x, L_y - 2\Delta l, z, t)}\right] \qquad \text{(Eq 13a)}$$

$$u = -V_B, \quad v = 0, \quad \text{and} \quad w = 0 \qquad \text{(Eq 13b)}$$

Boundary conditions on the yz-face at $x = 0$ and at time $t + \Delta t$ are:

$$T(0, y, z, t + \Delta t) = \max\left[T_A, \frac{T(\Delta l, y, z, t)^2}{T(2\Delta l, y, z, t)}\right] \qquad \text{(Eq 14a)}$$

where $x = 0$ does not coincide with the physical edge of the workpiece.

$$u = -V_B, \quad v = 0, \quad \text{and} \quad w = 0 \qquad \text{(Eq 14b)}$$

Boundary conditions on the yz-face at $x = L_x$ and at time $t + \Delta t$ are:

$$T(L_x, y, z, t + \Delta t) = \max\left[T_A, \frac{T(L_x - \Delta l, y, z, t)^2}{T(L_x - 2\Delta l, y, z, t)}\right] \qquad \text{(Eq 15a)}$$

$$u = -V_B, \quad v = 0, \quad \text{and} \quad w = 0 \qquad \text{(Eq 15b)}$$

It is important to note that the boundary conditions on the system boundaries at face xz at $y = L_y$, face yz at $x = 0$, and face yz at $x = L_x$ are physically consistent since in our calculations a solid state occurs in the neighborhood of these boundaries, that is, only if the temperature at grid points in the neighborhood of these boundaries is less than T_M so that $u = -V_B$.

5. Transition of SIMPLE Algorithm to a Quasi-Biharmonic Solver

According to the formalism of the SIMPLE algorithm, the *discrete* integral representation of the momentum transport equations, within the Boussinesq approximation, is:

$$U^{(n)}_{p,j} = \frac{1}{W_p}\left[\sum_{k=1}^{6} a_k U^{(n-1)}_{k,j} + \frac{\rho(\Delta l)^3}{\Delta t} U^0_{p,j}\right] + U^c_{p,j} \qquad \text{(Eq 16)}$$

where

$$W_p = \sum_{k=1}^{6} a_k + \frac{\rho(\Delta l)^3}{\Delta t} \qquad \text{(Eq 17)}$$

and $j = 1, 2$, and 3. The quantity $U^c_{p,j}$ is the correction term such that:

$$\sum_{i=1}^{3} \frac{\partial U_{p,i}}{\partial x_i} + \sum_{i=1}^{3} \frac{\partial U^c_{p,i}}{\partial x_i} = 0 \qquad \text{(Eq 18)}$$

The subscript p is the node index and the superscript (n) designates the value at the nth iteration. The weighting coefficients a_k and indexing scheme for node neighbors are defined in Ref 1. The quantity $U^o_{p,j}$ is the value of $U_{p,j}$ at the previous time step. A property of the coefficients a_k is that for sufficiently large μ:

$$a_k = \mu_k \Delta l \qquad \text{(Eq 19)}$$

Next, combining Eq 4 and 6, we obtain the governing equation of Stokes flow, that is:

$$\nabla^2 P = 0 \qquad \text{(Eq 20)}$$

Next, we note that:

$$\frac{\partial}{\partial x_j}(\nabla^2 P) = \nabla^2\left(\frac{\partial P}{\partial x_j}\right) \qquad \text{(Eq 21)}$$

For steady-state conditions:

$$\frac{\partial P}{\partial x_j} = \mu(T)\nabla^2 U_j \qquad \text{(Eq 22)}$$

Therefore:

$$\nabla^2(\mu(T)\nabla^2 U_j) = 0 \qquad \text{(Eq 23)}$$

or equivalently, via a finite-difference representation:

$$\mu_p \nabla^2 U_{p,j} = \frac{1}{6}\sum_{k=1}^{6} \mu_k \nabla^2 U_{k,j} \qquad \text{(Eq 24)}$$

where $\mu_k = \mu(T_k)$ and U_j is called a quasi-biharmonic function over the solution domain. Given the condition of geometric constraints and the mathematical conditions associated with the steady-state melt pool that are outlined in section 3, it follows from Eq 24 that:

$$U^{(n)}_{p,j} = \frac{1}{6\mu_p}\sum_{k=1}^{6} \mu_k U^{(n-1)}_{k,j} \qquad \text{(Eq 25)}$$

where the superscript (n) designates the nth iteration. A derivation of Eq 25 is given in Appendix 1. Note that in Eq 25 the coupling among $U_{k,1}$, $U_{k,2}$, and $U_{k,3}$ is through Eq 1. The presence of the function $\mu(T)$ in Eq 23 implies that U_j is not a biharmonic function in exact accordance with the mathematical definition, that is, $\nabla^4 U_j = 0$. However, within the approximation of small variations in the value of $\mu(T)$ with changes in the value of $\mathbf{x} = (x_1, x_2, x_3)$, which is consistent with the Boussinesq approximation, the functional character of U_j is very close to that of a biharmonic function and is therefore designated as quasi-biharmonic.

Equation 24 is a finite-difference representation of Eq 23, whose discretization is with respect to a uniform three-dimensional grid where the distance of separation between nodes is assumed to be sufficient for the specified tolerance. Comparison of Eq 25 and 16 shows that for steady-state conditions (or more generally for quasi-steady-state conditions), small Reynolds numbers, and a closed finite domain (whose boundaries are specified via geometric constraints on the flow field), the SIMPLE algorithm transitions to a quasi-biharmonic solver.

6. Sensitivity Analysis of Trailing Solidification Boundary

Reference 2 describes a procedure for imposing a melt-pool constraint at the top surface of the workpiece. This is effected by adjusting the values of the surface-tension-*like* coefficient defined by Eq 7. Although this coefficient has a formal similarity to that of a coefficient of surface tension, it no longer has this meaning. The coefficient defined by Eq 7 is for the purpose of *weighting* the velocity field at the top-surface plane so as to effect a geometric constraint on the melt pool that is consistent with experimental information about the shape of the solidification boundary that intersects the top-surface plane. The form of the modulation function $f_s(x,y)$ given in Eq 7 must be consis-

tent with the monotonicity conditions that follow from the physical character of the top-surface melt pool, these conditions being monotonicity relative to the center of the keyhole and monotonicity relative to the direction of motion of the beam. As indicated in section 3, the top boundary of the system represents a major influence on the character of the solution within the solution domain. Therefore, its accurate specification represents a key element of the method of using constraints.

In Ref 2 we presented a qualitative example of an adjustment of the shape of the top surface of the melt pool according to experimental measurements of the solidification boundary.

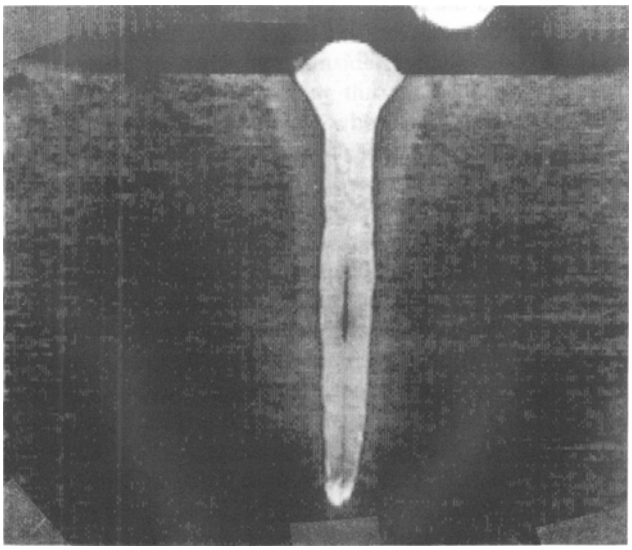

Fig. 2 Transverse cross section of weld showing penetration depth and transverse extent of melt pool. Figures 2 through 5 are cross sections corresponding to welds made under identical conditions.

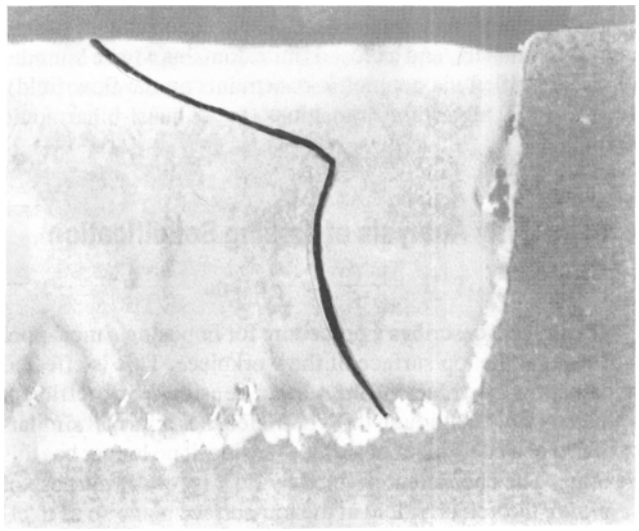

Fig. 3 Cross section of frozen solidification boundary corresponding to positive phase of harmonic perturbation of beam position

The underlying criterion for this particular type of geometric constraint on the flow field is that the two-dimensional solidification boundary at the top-surface plane can be accurately measured. In Ref 2 we also presented an inverse mapping procedure between an effective keyhole energy source and the trailing three-dimensional solidification boundary. The results of case study simulations given in that paper showed a high sensitivity of the steady-state trailing solidification boundary to changes in the shape of the effective keyhole boundary. This section describes results of case study analyses of the sensitivity of the trailing solidification boundary with respect to changes in conditions associated with the leading portion of the weld melt pool.

We consider first an experimental analysis of the sensitivity of the solidification boundary. A series of welds were performed under identical conditions (i.e., identical weld parameters). Typical cross sections for these welds are shown in Fig. 2 to 5. For these welds the beam is slightly defocused for the purpose of widening the weld and producing an exaggeration of the nail-head effect at the top surface. Superimposed on the beam motion relative to the workpiece is a small 60 Hz harmonic deflection. The amplitude of the harmonic deflection is on the order of 10^{-4} m. The harmonic component of the beam serves two purposes. One purpose is to provide a small perturbative deflection of the beam, which introduces a small harmonic variation in the cooling rate of the trailing section of the melt pool. This small variation of the cooling rate results in microstructure which, after polishing and etching, reveals the steady-state shape of the trailing solidification boundary. This is discussed further in section 8. Another purpose of the harmonic component of the beam is to provide a probe of the response of the trailing solidification boundary to changes in conditions at the leading part of the weld pool, that is, the *upstream* region of the melt pool near and including the keyhole.

The trailing edge of the solidification boundary intersecting the top-surface plane (see Fig. 5) was found to be weakly coupled to the harmonic variation of the leading edge of the melt

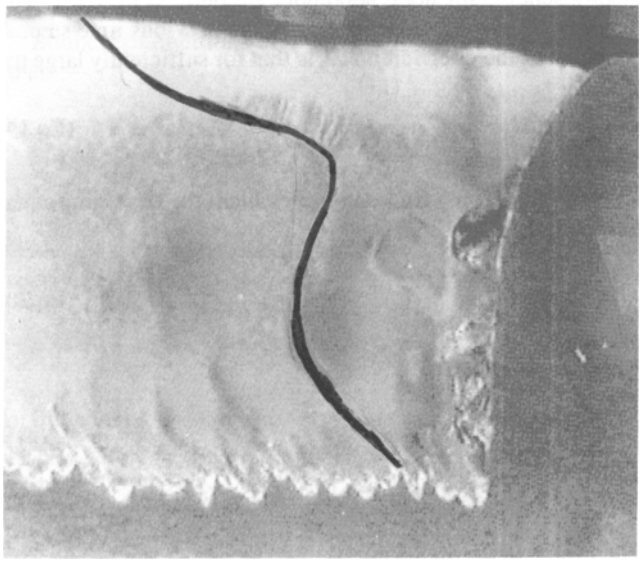

Fig. 4 Cross section of frozen solidification boundary corresponding to negative phase of harmonic perturbation of beam position

pool. That is, the shape of the two-dimensional top-surface trailing edge remained essentially constant. However, a strong coupling was observed between the harmonic variation of keyhole position below the top surface and the shape of trailing solidification boundary along the longitudinal section of the weld. This coupling is described by Fig. 3 and 4, which show cross sections of frozen solidification boundaries corresponding to positive and negative phases, respectively, of the harmonic variation of the beam position.

We consider next an analysis via numerical simulation of the sensitivity of the solidification boundary. The conditions on our model system are similar to those for our experimental analysis (e.g., the same welding speed V_B and penetration depth). For these simulations the modulation function $f_s(x, y)$ was adjusted according to the experimentally measured width of the top-surface solidification boundary (e.g., Fig. 5). Shown in Fig. 6 is the quasi-steady-state evolution of a melt pool initially at steady state. Referring to Fig. 6, it is seen that there is an increase in the length of the melt pool with time. This is due to the increase in energy that is input to the system, which is due in turn to the increase in the effective size of the keyhole. It is also observed that although there is coupling between the effective keyhole source and the trailing solidification boundary, the trailing solidification boundary is insensitive to the periodic

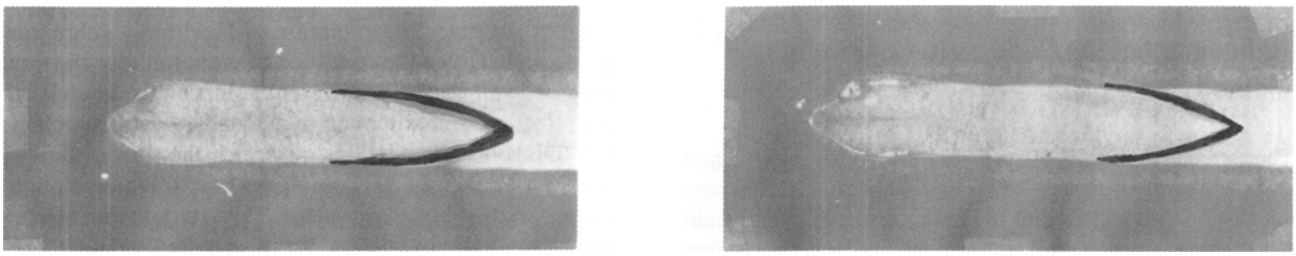

Fig. 5 Frozen solidification boundary intersecting top surface plane for two different welds made under identical conditions

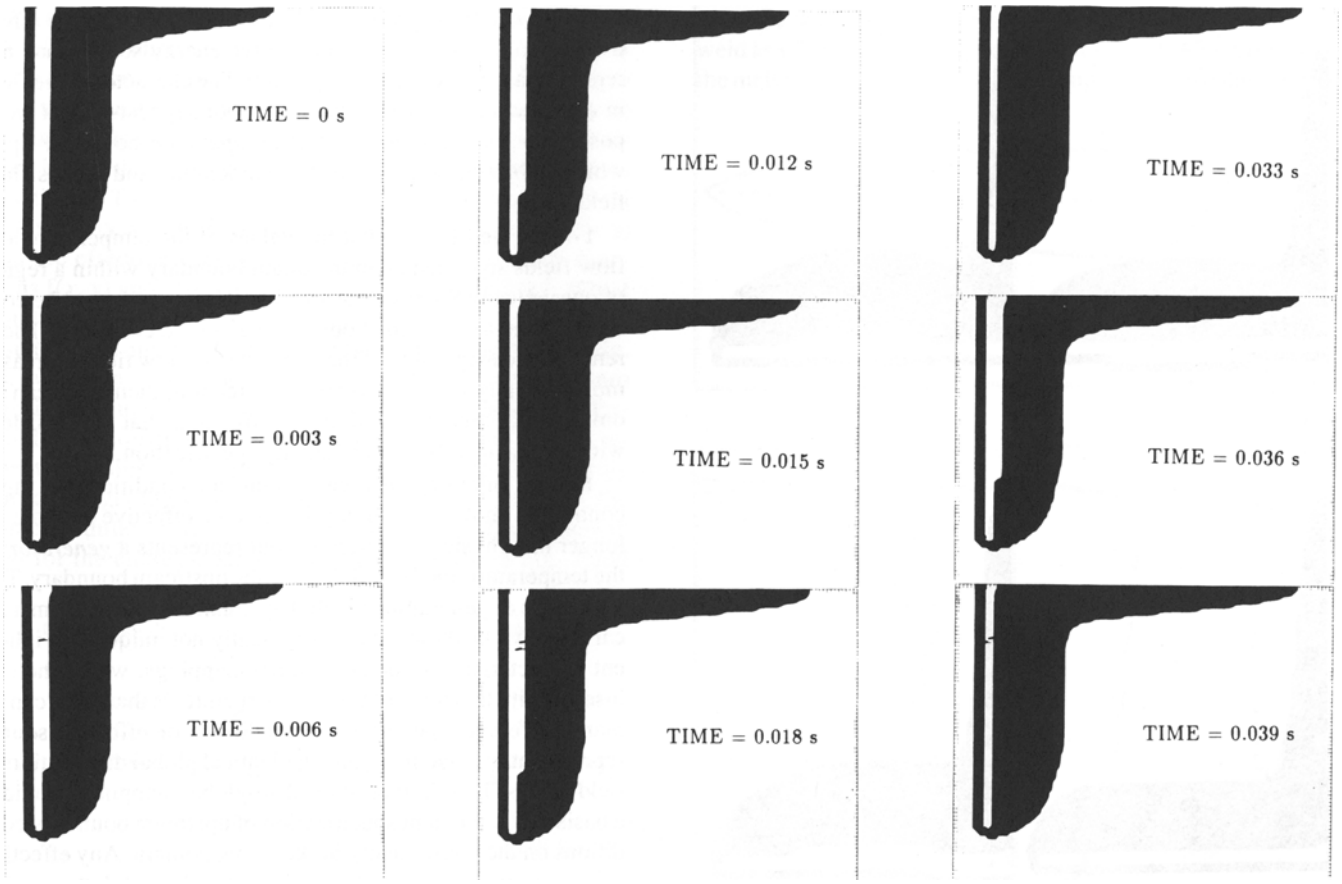

Fig. 6 Quasi-steady-state evolution of a melt pool to steady state resulting from oscillatory keyhole boundary. The initial shape of melt pool labeled TIME = 0.0 s is that corresponding to keyhole boundary labeled TIME = 0.003 s. At TIME = 0.0 s the keyhole boundary is turned on. The keyhole boundary, which is at 2740.85 °C, oscillates for a period of 0.006 s between each of the two different shapes shown.

changes in the energy source. That is to say, there is insensitivity to the details of change in shape of the keyhole boundary that occur over relatively short timescales. This suggests that the trailing solidification boundary couples only to the time-averaged keyhole.

Shown in Fig. 7 are steady-state melt-pool shapes corresponding to different effective keyhole sources. It can be seen that the shape of the trailing solidification boundary is relatively sensitive to the shape of the effective keyhole. This result is consistent with the experimental observation of a strong coupling between a variation of keyhole position below the top surface and the shape of the trailing solidification boundary (e.g., Fig. 3 and 4).

7. Refinement of the Geometric-Constraints Method

The present refinement of the geometric-constraints method (Ref 2) is based on the following mathematical properties which can be associated with the character of heat and fluid flow occurring in a melt pool resulting from a deep-penetration welding process. First, the solution domain defined by the melt pool resulting from a deep-penetration welding process includes subregions within which the flow of fluid is characteristically quasi-steady Stokes. This is especially true of regions of the trailing portion of the melt pool. A general property of quasi-steady Stokes flow is given by the following theorem (see page 132 of Ref 4 for proof).

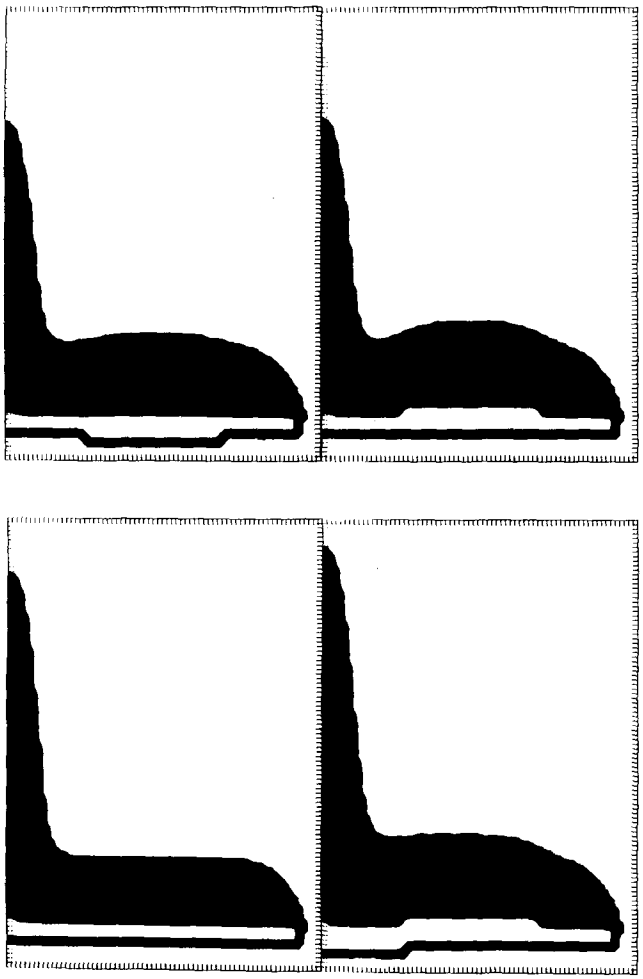

Fig. 7 Adjustment of effective keyhole source based on variation of shape of boundary of a given temperature

Theorem 1: There is a unique solution **U** of the equations governing the quasi-steady Stokes flow of incompressible fluid which satisfies prescribed boundary conditions.

Second, we observe that if within a boundary domain the solution **U** is known to be either monotonically decreasing or increasing, it is not necessary to have boundary value information over the entire boundary in order to effect a reasonably accurate determination of **U** within a subregion of the domain. Given the condition of monotonicity and a set of specified values of **U** at different points on the boundary, we can effect an approximation to a boundary value problem via constraints on the equations governing the flow of fluid. The condition of monotonicity provides a basis for interpolation between specified boundary values. This interpolation will represent a good approximation if the specified values of **U** are reasonably distributed.

Third, we observe that because the character of the flow in regions near the trailing solidification boundary is weakly coupled to the details of the character of the flow in regions near the keyhole (where the flow is not quasi-steady Stokes), an effective keyhole boundary or an effective energy source may not represent a well-posed *input* quantity. The character of the flow in *downstream* regions of the melt pool suggests that a well-posed input condition is that of an *upstream* boundary upon which are specified values of the temperature and Stokes-flow fields.

Fourth, we observe that the values of the temperature and flow fields specified at an upstream boundary within a region of quasi-steady Stokes flow are not arbitrary and must be consistent with *downstream* boundary values. According to Theorem 1, if the magnitude of the quasi-steady flow field decreases monotonically in the downstream direction, then there can be only one upstream boundary specification that is consistent with a given downstream boundary specification.

Finally, adopting upstream boundary conditions as input conditions on the system implies that the effective keyhole no longer has physical significance but represents a *generator* of the temperature and flow field over the upstream boundary. The procedure of generating a global upstream boundary from a local effective keyhole source is typically not unique. An inherent characteristic of local-to-global mappings, where there is insensitivity to details of the local structure, is that there can be many different types of local conditions or effective-source representations that map into an identical global distribution of field values. This feature of local-to-global mappings provides a basis for convenient specification of upstream boundary conditions on the quasi-steady Stokes-flow domain. Any effective source representation and associated local-to-global mapping is suitable if it generates upstream boundary values that are consistent with (or map into) specified downstream boundary values.

Given the above mathematical properties of the melt pool and interrelation between its subregions, a specific approach for applying the procedure for calculating the temperature and flow fields according to the geometric constraints method can be effected. In detailing this approach, we refer to Fig. 8, which gives a two-dimensional schematic description of the partitioning of the weld melt pool into two subregions. One subregion consists of fluid whose flow character is only quasi-steady Stokes. The other subregion contains the keyhole and consists of fluid whose flow character is not that of quasi-steady Stokes. Although Fig. 8 shows only a two-dimensional top-surface cross section of a melt pool, the present discussion concerns the entire three-dimensional melt pool.

The initial step of the procedure for calculating **U** and T is to specify a relatively well-distributed set of downstream boundary values. An example of this set of values is shown in Fig. 9, which illustrates the maximum separation between the center of the beam energy source and the trailing solidification boundary along the top surface of the workpiece (C_1), the lateral cross section of the weld that is perpendicular to the direction of travel of the beam (C_2), and the solidification curve corresponding to the intersection of the trailing solidification boundary and the plane passing through the center of the beam and parallel to the direction of beam travel (C_3). A general discussion concerning the extraction of curves C_1, C_2, and C_3 is given in section 8.

The next step of the procedure is the selection and adjustment of the modulation function $f_s(x, y)$ defined by Eq 7 and of the effective energy source. The criterion for adjustment of these functions is *not* the generation of a temperature and flow field that generate the entire solid-liquid boundary defining the dynamic weld melt pool. The criterion for adjusting these functions is only that a specified set of downstream boundary values is satisfied. This less restrictive criterion provides a high level of flexibility with respect to adjustment and selection of $f(x, y)$ and the effective energy source. Any combination of functions $f(x, y)$ and effective energy sources is sufficient if that combination generates boundary values on the upstream boundary of the quasi-steady Stokes flow region (see Fig. 8), which in turn generates **U** and T fields that map into specified boundary values on the downstream boundary. Examples demonstrating the high level of flexibility with respect to adjustments of $f(x, y)$ and the effective energy source are given by Fig. 7 and 10. For both Fig. 7 and 10, the same modulation function $f(x, y)$ is adopted. It is assumed that for the energy-source adjustments shown in Fig. 7 and 10 one is seeking T and **U** fields that would satisfy downstream boundary values such as are given by curve C_3 in Fig. 9. In Fig. 7, adjustment of the energy source is effected by variation of the shape of a surface having a fixed temperature (i.e., T_G). As can be seen, many of the qualitative features of curve C_3 in Fig. 9 can be obtained via simple changes in the shape of the surface. Quantitative agreement in accordance with specified downstream-boundary values would, of course, require more detailed changes in the shape of the surface. In Fig. 10, adjustment of the energy source is effected by variation of the temperature of a surface having a fixed shape.

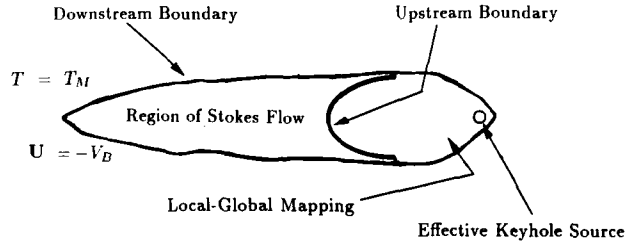

Fig. 8 Top-surface schematic description of the partitioning of weld melt pool into a subregion where the flow of fluid is quasi-steady Stokes and a subregion containing an effective energy source.

8. Method of Extracting Experimental Information for Constraining the U and T Fields

Given the unavailability or difficulty of obtaining experimental information relating to the shape of the melted region during a deep-penetration welding process, it is necessary to investigate methods of extracting this information after the weld is completed. In principle, this information is readily available through common metallographic analysis of welds as is typically performed using specialized preparation techniques. Generally, the information extracted from a weld is obtained from the transverse view of the weld cross section. This view provides the depth of penetration, the transverse width of the weld as a function of depth, and a view of the HAZ surrounding the melt region (e.g., Fig. 2). A longitudinal view of the weld FZ

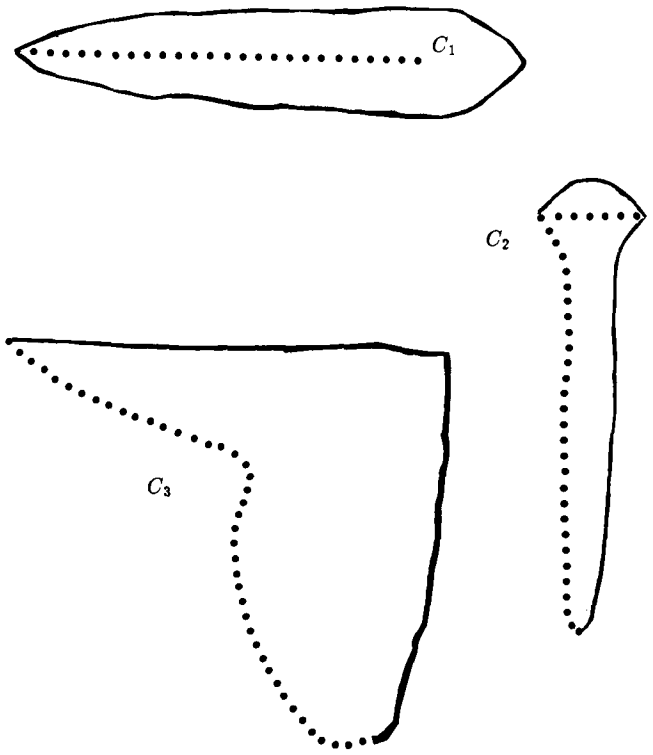

Fig. 9 Example of a set of downstream boundary values obtained from experimental measurements

along the centerline of the weld is sometimes examined for the presence of weld discontinuities over a length of weld section. The short-transverse top view of the weld is usually examined optically for the presence of cracks or undercuts at the top edge of the weld boundary and to determine the condition of the top bead. Grinding, polishing, and etching of the top view of the weld is often not performed.

In practice, elimination or minimization of the weld crater is effected by a controlled reduction of the weld process parameter affecting *downsloping* of the melt pool. Rarely is there an examination of the weld crater that is caused by an abrupt discontinuation of the heat input. The weld crater is considered undesirable and eliminated in practice. It is also considered unrepresentative of the dynamic steady-state conditions of a weld and therefore often ignored as a source of information related to these conditions. However, the *coupling* between the short-time transient response of the melt pool, which follows an abrupt discontinuation of the heat input from either an electron or laser beam, and the rapid rate of solidification of high-aspect-ratio beam welds provides the basis for a method of extracting experimental information related to the dynamic steady state of the melt pool. This method entails inspection of the weld crater to reveal additional information representative of dynamic steady-state conditions of the deep-penetration welding process.

We have observed that experimental information which is not typically gathered from common metallographic weld sectioning is available and is representative of the dynamic steady state of the melt pool. This experimental information includes the shape of the melt pool in the top section of the weld and the shape and extent of the melt pool along the centerline of the weld. This information can be obtained quantitatively along with the commonly obtained data of weld penetration and width as a function of depth.

A procedure for obtaining this information is as follows. First, weld samples are prepared for examination by initiating in each case a weld, allowing the weld to reach a steady state for a given set of process parameters, and then abruptly discontinuing the weld schedule. Metallographic sectioning is performed in such a way as to include within each top, transverse, and longitudinal view both a steady-state region of the weld and a region containing the weld crater. In order to obtain the three different views from a single weld, the top view must be prepared and examined before the longitudinal view. Preparation of the longitudinal view for examination requires removal of half of the top view. Cutting, etching, and polishing are performed to reveal the features of interest. The choice of etchant is critical with respect to revealing the features of interest in each of the different views. In the case of stainless steel, Marble's reagent is used to examine macrofeatures that are not ob-

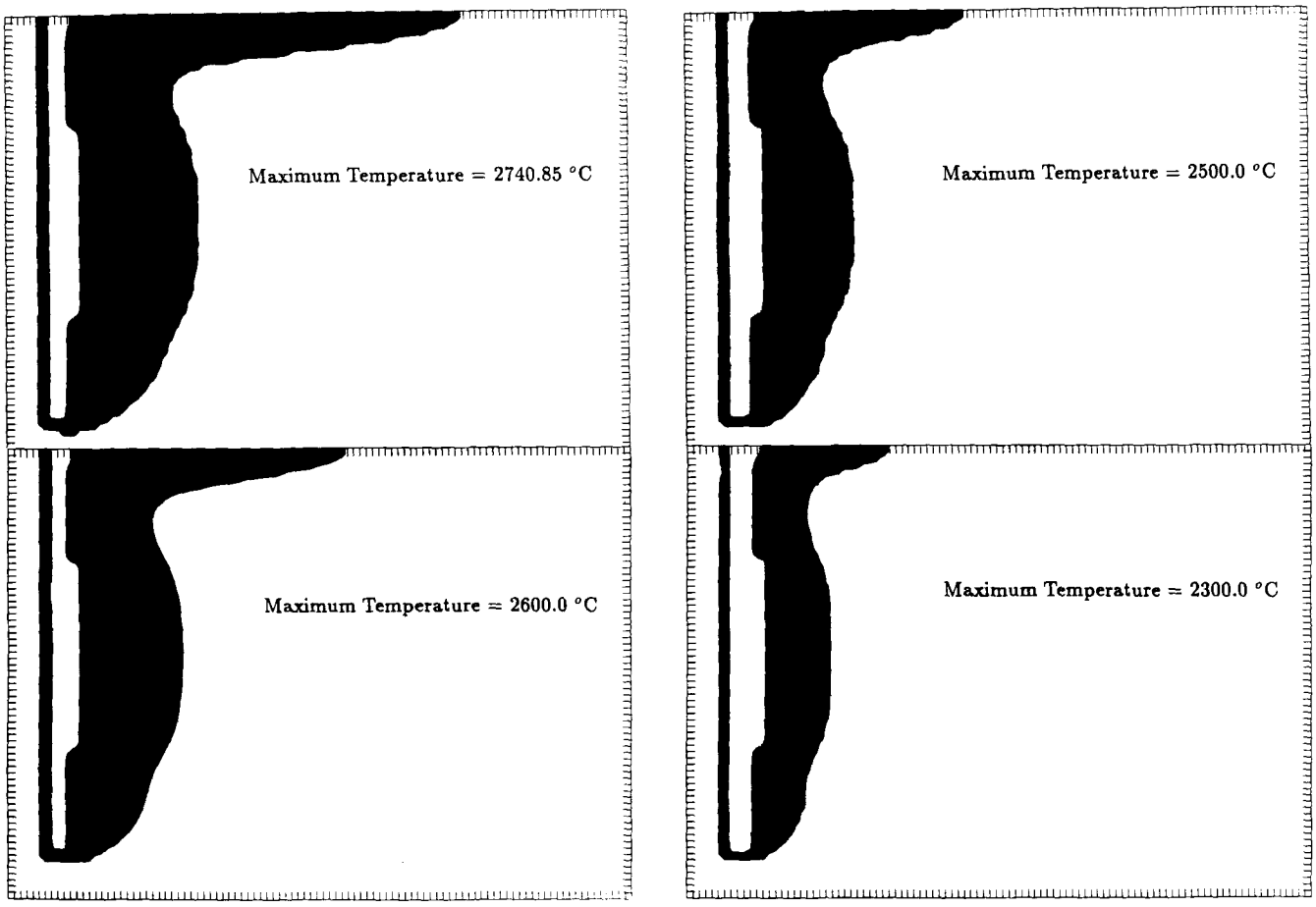

Fig. 10 Adjustment of effective keyhole source based on variation of temperature of boundary of a given shape

servable with an etchant typically used to examine weld microstructure (e.g., Fig. 11). In the case of partial-penetration-beam welds, where an amount of material usually flows and solidifies above the top surface of the material, the preparation of the top view of the weld includes removal of this material by grinding smooth to the top surface of the material. The top view of the weld crater can be used to define the length, width, and shape of the weld melt pool at the time of discontinuation of heat input.

In the case of high-energy-density welding (e.g., laser or electron-beam welding), the discontinuation of energy input to the system is sufficiently abrupt that most of the dynamical features of the system are *frozen* into the macrostructure of the solidified system. Following the abrupt termination of driving forces due to the beam-material interaction, solidification of the system occurs with minimal disturbance and over a time period that is on the order of microseconds. Evidence of how quickly the system freezes is shown in Fig. 11, where horizontal flow patterns within a section of the keyhole are readily observed, indicating the precise condition of the keyhole wall at the time the beam energy input was discontinued.

During the dynamic steady state of the weld, oscillations in fluid flow and of the keyhole can be readily observed using electron-beam welder viewing optics at 40× magnification. Accordingly, slight oscillations of the trailing solidification boundary of the weld can be observed. When the beam energy input is abruptly discontinued, solidification still progresses to completion, but without any of the interruptions associated with the driving forces in the fluid due to the beam-material interaction. During the dynamic steady state of the weld melt pool, any small oscillations or in general any small temporal variations of the trailing solidification boundary are manifested as changes in the cooling rate of this boundary. These slight changes in the cooling rate are observable in the microstructure of the solidified weld zone by changes in the relative volume of primary and secondary phases and in grain size.

As a result, macrostructural patterns can be formed, such as the solidification banding shown in Fig. 11. These patterns reveal the entire shape of the solidification boundary existing during the dynamic steady state of the weld melt pool. One is able to observe, effectively, the extent of the trailing solidification boundary at the instant of time the beam energy input is discontinued. This quantity is revealed by the condition of *uninterrupted* solidification and *bandless* microstructure that progresses from the farthest extent of the weld melt pool, at the trailing solidification boundary, to the region of the melt pool having solidified last. A quantitative measurement of this unbanded region provides information about the extent of the melt pool during the dynamic steady state (e.g., curve C_1 in Fig. 9). One should note, however, that our technique relies heavily on the characteristic change in etching rates, which is in turn due to slight changes in the microstructure of the material studied (i.e., duplex stainless steel). The applicability of the technique to other materials remains an open question.

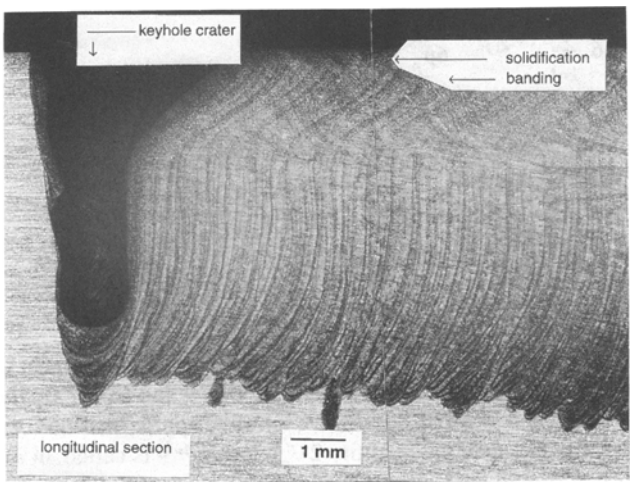

Fig. 11 Longitudinal view of frozen dynamical features of weld, including flow within the keyhole and the trailing solidification boundary.

The technique described is also applicable for determining the shape of the solidification boundary along the *longitudinal section* of the weld—for example, curve C_3 in Fig. 9, where a similar banding effect is observed. Although not as pronounced as in the top surface of the melt pool, banding can be observed along the longitudinal section of the weld that is representative of the shape of the trailing solidification boundary.

One can, in principle, superimpose a specified type of temporal variation on the shape of the keyhole in order to induce variations in the solidification rate of the trailing boundary, which is in turn revealed in the microstructure by the technique described (e.g., Fig. 3 and 4). However, in practice there is already associated with the keyhole sufficient quasi-periodic or intermittent character for inducing variations in the solidification rate.

We indicate that our method of extracting information about the shape of the trailing solidification boundary is with respect to a different sensitivity regime than that considered by the analysis described in section 6 of this paper. Although there is a coupling between changes in the keyhole and the detailed character of the microstructure at the trailing solidification boundary, these temporal changes are not coupled to boundary shape. The characteristic scale of resolution of the model system defined by Eq 1, 4, and 6 is macroscopic. The insensitivity of the trailing solidification boundary to details of the character of the beam energy source is a macroscopic property of the dynamic weld melt pool. It is the macroscopic shape of the trailing solidification boundary that represents geometric-constraint information.

9. Conclusions

In one sense our approach represents an extension of the methods that employ a phenomenological heat source moving through a solid whose parameters are adjusted such that the calculated temperature of solidification (or liquefication)—that is, T_M—isotherm matches experimental measurements (Ref 8). Our approach entails the specification of upstream boundary values of the temperature fields and flow fields that are such that downstream boundary values match experimental measurements. However, our approach differs from those that employ a phenomenological heat source since it entails a complete accounting of all the physical transport: mass, energy, and momentum. Because of this distinct feature, adjustment of up-

stream boundary values in accordance with experimental measurements does not represent an arbitrary-parameter adjustment. The mathematical properties of a bounded quasi-steady Stokes-flow region ensure that there exists only one set of upstream values of T and $\mathbf{U}$ that is consistent with a given set of downstream boundary values, that is, the solidification boundary. Therefore, our refinement of the geometric-constraints method, which was originally introduced in Ref 2, entails a deemphasis of upstream boundary information that is outside the quasi-steady Stokes-flow region of the weld melt pool.

An extension of our approach should be the inclusion of geometric information associated with expansion or flow of liquid above the plane corresponding to the top surface of the workpiece. Our refinement of the geometric-constraints method presented here has adopted the top-surface plane of the workpiece for specification of top-surface boundary values of T and $\mathbf{U}$. This surface, however, does not correspond to the physical top-surface boundary of the melt pool. It remains an open issue for further investigation to determine to what extent inclusion of information concerning the physical top-surface boundary provides a basis for a complete specification of the system via a relatively small set of boundary values extracted from experiment. For example, which among the different types of boundary values shown in Fig. 9 are no longer necessary for a complete specification of the system if boundary values associated with the physical top surface of the melt pool are included?

We wish to indicate explicitly that our method is not limited only to the prediction of the temperature field in the solid, including the HAZ. One may infer, incorrectly, that adopting a set of upstream boundary values of the temperature and flow field rather than an explicit representation of the keyhole energy source implies an inherent approximation of the T and $\mathbf{U}$ fields within the liquid region. In principle, our approach provides a complete specification of the temperature field in the solid, including the HAZ, and of the temperature and flow field $\mathbf{U}$ in the FZ for regions of the melt pool close to the solidification boundary—or, more precisely, for regions of the FZ for which the character of the fluid flow is quasi-steady Stokes.

Acknowledgments

The authors would like to thank Dr. Edward A. Metzbower and Mr. Harry Jones III for their discussions.

Appendix 1: Iterative Solution of Biharmonic Equation with Constraints

There is a unique solution of Eq 23 within a finite closed domain if U_j, ∇U_j, $\nabla^2 U_j$, and $\nabla^3 U_j$ are specified over a finite region, including the boundary, enclosing the domain. We note that this condition is not the same as $\nabla^n U_j$, $n = 0$, 1, 2, and 3, specified *at* the boundary. For this type of specification, a unique solution does not exist (Ref 9). Equivalently, via a finite-difference representation, there is a unique solution of Eq 24 within a finite closed domain if the value of U_j is specified at all nodes within four internode separations from the boundary nodes. This condition is imposed implicitly by imposing geometric constraints of the flow field. We note that given the above condition on the boundary nodes and their near-neighbor nodes, Eq 25 can be derived from Eq 24. From Eq 24, it follows that:

$$U_{p,j} = \frac{1}{6\mu_p} \sum_{k=1}^{6} \mu_k U_{k,j} - \frac{(\Delta l)^2}{36\mu_p} \sum_{k=1}^{6} \mu_k \nabla^2 U_{k,j} \qquad \text{(Eq A1)}$$

Next, for the second term of Eq A1, there is the identity:

$$\frac{1}{36\mu_p} \sum_{k=1}^{6} \mu_k \nabla^2 U_{k,j} = \frac{1}{6} \nabla^2 \left[\frac{1}{6\mu_p} \sum_{k=1}^{6} \mu_k U_{k,j} \right] = \frac{1}{6} \nabla^2 \langle U_{p,j} \rangle \qquad \text{(Eq A2)}$$

where

$$\langle U_{p,j} \rangle = \frac{1}{6\mu_p} \sum_{k=1}^{6} \mu_k U_{k,j} \qquad \text{(Eq A3)}$$

and

$$\nabla^2 \langle U_{p,j} \rangle = \sum_{k=1}^{6} \langle U_{k,j} \rangle - 6 \langle U_{p,j} \rangle \qquad \text{(Eq A4)}$$

Combining Eq A1, A2, and A3, it follows that:

$$U_{p,j} = \frac{2}{6\mu_p} \sum_{k=1}^{6} \mu_k U_{k,j} - \frac{1}{6} \sum_{k=1}^{6} \langle U_{k,j} \rangle \qquad \text{(Eq A5)}$$

Next, we note that:

$$\frac{1}{6} \sum_{k=1}^{6} \langle U_{k,j} \rangle \approx \frac{1}{6\mu_p} \sum_{k=1}^{6} \mu_k \langle U_{k,j} \rangle \qquad \text{(Eq A6)}$$

which, when substituted into Eq A5, gives:

$$U_{p,j} = \frac{1}{6\mu_p} \sum_{k=1}^{6} \mu_k \left[2U_{k,j} - \langle U_{k,j} \rangle \right] \qquad \text{(Eq A7)}$$

The quantity $2U_{k,j} - \langle U_{k,j} \rangle$ has significance with respect to the process of iteration. In general, if $U_p^{(n-2)}$ and $U_p^{(n-1)}$ are the $(n-2)$th and $(n-1)$th successive iterative approximations of a quantity U_p, then the quantity $2U_p^{(n-1)} - U_p^{(n-2)}$ is called an *extrapolation to the root* and is an estimate of the nth iterate $U_p^{(n)}$ (Ref 10). The equivalence between Eq A7 and 25 follows by noting that the quantity $U_{k,j}$ represents a successive iteration with respect to the quantity $\langle U_{k,j} \rangle$.

Appendix 2: Model Parameters and Physical Quantities

$T_M = 1426.85\ °C$ $T_G = 2740.85\ °C$ $V_B = 0.03\ m/s$

$\Delta l = 10^{-4}\ m$ $\Delta t = 5 \times 10^{-4}\ s$

$L_x = 10^{-2}\ m$ $L_y = 4 \times 10^{-3}\ m$ $L_z = 7 \times 10^{-3}\ m$

References

1. S.G. Lambrakos, E.A. Metzbower, P.G. Moore, J.H. Dunn, and A. Monis, *J. Mater. Eng. Perform.*, Vol 2 (No. 6), 1993, p 819
2. S.G. Lambrakos, E.A. Metzbower, J. Milewski, G. Lewis, R. Dixon, and D. Korzekwa, Simulation of Deep Penetration Welding of Stainless Steel Using Geometric Constraints Based on Experimental Information, *J. Mater. Eng. Perform.*, Vol 3 (No. 5), 1994, p 639
3. M.E. O'Neill and F. Chorlton, *Ideal and Incompressible Fluid Dynamics*, John Wiley & Sons, 1986
4. M.E. O'Neill and F. Chorlton, *Viscous and Compressible Fluid Dynamics*, John Wiley & Sons, 1989
5. E.M. Sparrow, S.V. Patankar, and S. Ramadhyani, *Trans. ASME*, Vol 520 (No. 99), 1977
6. S.V. Patankar, *Numerical Heat Transfer and Fluid Flow*, Hemisphere Publishing, 1980
7. D. Zwillinger, *Handbook of Differential Equations*, Academic Press, 1989 (see p 514, 579)
8. E.A. Metzbower, *Weld. J.*, Vol 69 (No. 7), 1990, p 272
9. J.D. Jackson, *Classical Electrodynamics*, John Wiley & Sons, 1962 (see p 15 for discussion)
10. E. Isaacson and H.B. Keller, *Analysis of Numerical Methods*, John Wiley & Sons, 1996 (see p 374 for discussion)